5-1-2022

A dynamic co-simulation framework for the analysis of battery electric vehicle thermal management systems

T. Shelly

Justin A. Weibel
jaweibel@purdue.edu

D. Ziviani

E. A. Groll

2022 21st IEEE Intersociety Conference on Thermal and Thermomechanical Phenomena in Electronic Systems (iTherm) | 978-1-6654-8503-6/22/$31.00 ©2022 IEEE | DOI: 10.1109/iTherm54085.2022.9899690

A Dynamic Co-Simulation Framework for the Analysis of Battery Electric Vehicle Thermal Management Systems

Tayler Shelly
Purdue University
Mechanical Engineering
West Lafayette, USA
tshelly@purdue.edu

Justin A. Weibel
Purdue University
Mechanical Engineering
West Lafayette, USA

Davide Ziviani
Purdue University
Mechanical Engineering
West Lafayette, USA

Eckhard A. Groll
Purdue University
Mechanical Engineering
West Lafayette, USA

***Abstract*— At high charging and discharging rates, batteries are typically dominated by high rates of ohmic heating which poses a problem for decreasing charge times of consumer battery electric vehicles (BEVs). This problem inherently deals with multi-physics phenomenon at varying scales from vehicle-level thermal management systems down to cell construction and Li-ion transport. This study develops a co-simulation framework for the analysis of a battery electric vehicle thermal management system (TMS) that couples a dynamic system-level model (Modelica) with a high-fidelity finite volume battery module thermal model (COMSOL). The thermal management system investigated is one incorporating waste heat recovery (WHR) suited for high capacity BEVs operating over long range cycles, which harvests waste heat from power electronics for use in cabin or battery heating. A novel co-simulation control scheme is developed, characterized, and shown to provide improvements to instantaneous and cumulative error across the simulated cycle. As a result of the present study, a holistic co-simulation framework is developed, tested, and various case studies of a parameterized battery pack are shown. Future work will extend this to battery aging characterization and lifetime technoeconomic study considering BEV thermal management system components.**

Keywords—Fast Charging, Co-Simulation, Battery Electric Vehicle, Thermal Management

I. NOMENCLATURE

$\boldsymbol{a}$	Correlation coefficient for cell degradation
$\boldsymbol{C}$	Compressor or Charge rate (1/h)
$\boldsymbol{CD}$	Charge discharge binary value
$\boldsymbol{c_p}$	Specific heat at constant pressure (kJ/kg-K)
$\boldsymbol{E}$	Activation energy (kJ/K*mol)
$\boldsymbol{F}$	Fan
$\boldsymbol{I}$	Current (A)
$\boldsymbol{P}$	Pump
$\boldsymbol{R}$	Resistance (Ohm)
$\boldsymbol{t}$	Time (s, h)
$\boldsymbol{\Delta t}$	Co-simulation time step (s)
$\boldsymbol{u}$	Input
$\boldsymbol{v}$	Velocity (m/s)
$\boldsymbol{V}$	Valve or Voltage (V)

Greek Symbols

ρ	Density (kg/m^3)
Σ	Continuous summation

Subscripts

$\boldsymbol{c}$	Capacity loss
$\boldsymbol{f}$	Final value
$\boldsymbol{inc}$	Increase
int	Effective internal resistance model
$\boldsymbol{loss}$	Loss
$\boldsymbol{o}$	Initial value
$\boldsymbol{r}$	Power fade
$\boldsymbol{SIM}$	True simulated value
$\boldsymbol{TISC}$	Co-simulated value
1,N	Discretized co-simulation step size values

Acronyms

APM	Auxiliary power module
BEV	Battery electric vehicle
CC-CV	Constant current constant voltage
EM	Electric motor
EOC	End of charge condition
EOD	End of discharge condition
ESS	Energy storage system
EXV	Electronic expansion valve
HVAC	Heating, ventilation, and air conditioning
HX	Heat exchanger
OCV	Open circuit voltage
PTC	Positive temperature coefficient
TMS	Thermal management system
TPIM	Traction power inverter module
WHR	Waste heat recovery

II. INTRODUCTION

Electrification of the vehicle fleet via consumer adoption of battery electric vehicles (BEVs) is hindered by range and range anxieties, cost, and lifetime performance of these vehicles. To investigate and improve each of these BEV thermal management systems (TMSs) are being continuously investigated and optimized in research and commercial solutions alike with key metrics being system range, battery aging, and overall system cost. Often these studies focus on evaluating specific components of the TMS, such as the cabin, power electronics, or battery thermal management. As exhaustively

reviewed previously [1], examples of these include studies on the effect of cooling channel optimization and pack construction on cell temperature gradients, which seek to optimize for battery cell thermal performance. Such component-level studies must typically assume some boundary conditions at the interface to the vehicle-level TMS, which are either held constant or varied parametrically to characterize the response of the battery temperatures. The type of battery management system can also be varied to investigate and optimize for battery thermal performance [2]. The same component-level investigation approach is also typical for cabin heating, ventilation, and air conditioning (HVAC) systems, with optimization of the BEV TMS for heat pumping [3], combined fluid loop thermal management [4], and investigations of different refrigerant types for extreme conditions [5]. Each of these studies must make various simplifications to other aspects of the thermal management, such as neglecting the presence of the power electronics or battery systems entirely [3, 5], or simplifying them to point sources of heat in the HVAC system [4]. These simplifications appropriately serve the original purposes of these studies but leave open investigations into the effect of the TMS on the aging performance of cells. Studies investigating battery aging performance have been completed with relatively simplified thermal models that assume the battery to be at constant temperature [6, 7] or establish a resistance network [8] for thermal calculations. This has set a precedent for making significant simplifications to the TMS, using reduced-order assumptions, to support all previous investigations into aging of batteries.

The goal of this study then is to establish a full BEV TMS model representing all salient components that is coupled with a 3D finite volume battery module thermal model, as a co-simulation platform for investigation of battery aging. This builds off the previous works of the authors [9, 10] which investigated the long-range EV thermal management system performance as a function of ambient conditions and system architecture. The two modeling environments are first established separately and then the necessary interconnections to allow co-simulation are created. These interconnections include derivative-controlled adaptative co-simulation step sizes based on the vehicle velocity and mode of system operation, battery charging and discharging controllers, and a velocity profile controller to start and stop the vehicle corresponding to charging behavior. Finally, a case study of long-range BEV performance is co-simulated to illustrate each functional aspect of the parameterized co-simulation scheme. This result has implications for future work investigating the technoeconomic performance and aging of battery cells as a function of the BEV TMS design.

III. Modeling Methodology

The following subsections introduce the thermal system and battery models, co-simulation framework, and simulation control parameters. The software used for the dynamic thermal system model is Modelica running on Dymola [11]. For Modelica, TLK libraries are used encompassing TIL 3.10 and TISC 2.8.0 [12]. Finite volume thermal simulation of flow and heat transfer in the battery module is performed using COMSOL Multiphysics 5.6 [13].

A. Vehicle thermal management system model

Our past efforts developed a model of a full BEV TMS with waste heat recovery (WHR) in Refs. [9, 10] . The primary operational modes of this system are briefly summarized below based on the schematic diagram shown in Fig 1. Readers are referred to our past studies for all further details about the subcomponents and model implementation. All key assumptions in the thermal system model remain the same as from this past work, with a few notable exceptions described in the coming sections, including the system control and the assumed battery model. The heat transfer correlations inside of the system are the same as previous works except for the refrigerant-side correlations in the vapor compression cycle (VCC), which are changed to a blended correlation for condensation [14] and evaporation [15]. In Fig 1 the boundary between the overall thermal system model and the finite volume battery module model are indicated by a red dashed line.

The cycle has three discrete possible modes of operation: discharging and heating, discharging and cooling, or charging mode. In discharging and heating mode the TMS architecture layout enables the recovery of waste heat from the power electronics for heating the cabin or battery environment via two four way valves (V5, V6). With these, the water glycol loops can be placed into either series, such that all glycol loops share common heat sources, or parallel configurations where the loops are then independent. For the purposes of this study only the latter two modes, discharging and cooling or charging, occur under the conditions and velocity profile investigated.

During discharging and cooling, starting from the compressor (C1) outlet in the refrigerant (R134a) line, superheated refrigerant enters the vehicles front end heat exchanger. A fan, F1, blows air over this exchanger to condense and subcool the refrigerant as it exits to a branch point with two

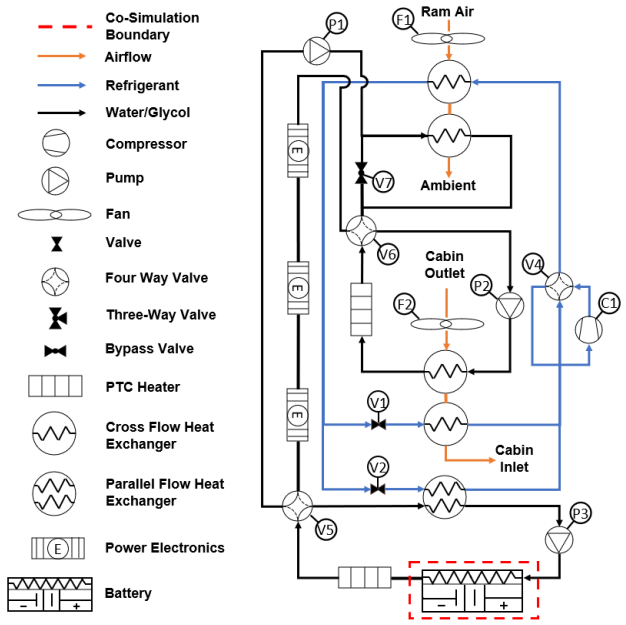

Fig 1: Battery electric vehicle thermal management system with waste heat recovery.

system expansion valves (EXV). The cabin EXV, V1, expands the refrigerant to a lower pressure and into the cabin heat exchanger, an evaporator in this case. The evaporating refrigerant cools the air pushed over the exchange by fan F2. Then, through closed-loop control of V1 and the compressor, the superheat at the exit of the evaporator and the cabin inlet temperature are controlled, respectively. Returning to the EXV branch point, V2 expands refrigerant flow while controlling for the battery module inlet temperature. The expanded refrigerant then passes through a battery heat exchanger that is sufficiently sized to ensure a superheated exit state. Both the cabin and battery refrigerant lines mix before entering back in the compressor. Moving next to the water/glycol loops inside of the system under the same operating mode, these are all separated using four-way flow control valves V5 and V6. Starting at P1, water glycol is pumped through a front-end heat exchanger which removes heat from the traction drive power electronics inside of the system. For cabin heating. a loop of water/glycol, heated via a positive temperature coefficient (PTC) heater, is circulated via pump P2. Finally, pump P3 circulates the water/glycol used for heating or cooling of the battery.

In the charging mode, it is assumed that the vehicle is stationary, and the cabin is conditioned. Thus, V1 remains closed and the compressor controls for battery inlet temperature while V2 controls for superheat at the inlet to the compressor. The fans and pumps for cooling power electronics and the cabin environment are shut off.

B. Battery electric, aging, and thermal models

With the goal of co-simulation, a high-fidelity model of thermal transport in the battery module and cold plate is established to calculate the heat transfer performance, battery temperature distribution, and local state of health (SOH). A battery cell model is selected from the literature [16] which accounts for power (R_{inc}) and capacity (C_{loss}) fade as a function of battery throughput (Ah), temperature (T), and charging rate (CR)

$$C_{loss} = \left(a_C(SOC_{min}) * \exp\left(-\frac{E_{a_C}}{R_g T}\right) * Ah^z\right) * \frac{C_o}{100} \quad (1)$$

$$R_{inc} = \left(a_R(SOC_{min}, CR) * \exp\left(-\frac{E_{a_R}}{R_g T}\right) * Ah\right) * \frac{R_o}{100} \quad (2)$$

Here E_{a_C} and E_{a_R} are the cell activation energy for capacity and power fade respectively, R_g is the universal gas constant, SOC_{min} is the minimum state of charge for the model set in this case to 0.25, and z is a fitting coefficient set to 0.48. In this study, a fast charge rate of 5C is considered. The coefficients of capacity fade, a_C, and resistance increase, a_R, are calculated according to known parameters and coefficients from the original literature source [16]. The chosen cell is a 15 Ah capacity prismatic cell with a nominal voltage of 3.7 volts. Key thermal properties and geometric parameters of the battery cells are shown in Table 1.

With the characteristics of a single cell specified, a battery pack is designed to achieve a 95 kWh capacity at 400 V. Given the cell voltage of 3.7 V, this target pack voltage fixes the number of cells chained in series at 108 cells. This then requires 16 such cell-chains connected in parallel to achieve the necessary pack capacity of approximately 95 kWh. Uniform volumetric heat generation in each cell is based on adopted battery parameterization data [16] in the form of an effective internal resistance (R_{int}) circuit model. Heat generation is governed by ohmic heating of the battery across R_0, the initial value for ohmic resistance of the battery cell, with the addition of any accumulated power fade as.

Table 1:Thermal properties and geometric parameters of the battery cell.

Parameter	Value	Unit
$length$	0.241	m
$width$	0.165	m
$thickness$	0.00625	m
$mass$	0.383	kg
ρ	1541	kg/m^3
c_p	1050	kJ/kg-K

$$Q = I^2(R_0 + R_{inc}) \quad (3)$$

Coulomb counting is employed to track the batteries SOC at any given instant as a function of the capacity loss subtracted from the initial system capacity

$$SOC(t) = SOC(t_0) - \int_{t_o}^{t} \frac{I}{(C_o - C_{loss})} dt \quad (4)$$

where t is measured in hours for appropriate dimensions with the traditionally defined battery capacity in amp hours. This formulation ignores polarization losses and entropic losses due to the lack of available data from open literature sources.

Utilizing the calculated number of cells, the battery thermal model is constructed for a single chain of 108 cells in series. Coolant flows through a cold plate across the bottom of the cells; it is thereby inherently assumed that that total coolant flow in the thermal system is equally distributed among 16 parallel such flow paths. In the pack construction, one conducting fin is placed between pairs of two battery cells (i.e., such that only one side of each cell contacts a fin, with the other side facing a TIM and battery cell face.). This is shown in Fig 2 with a zoomed inset view for additional detail. A thermal contact resistance value of 300×10^{-6} m^2*K/W [17] is used for all interfacial gaps in the battery module, between the coldplate and fins, batteries and the fins, and between the batteries themselves. This corresponds to an equivalent material thickness of 1 mm at an effective thermal conductivity of 3.33 W/(m-K).

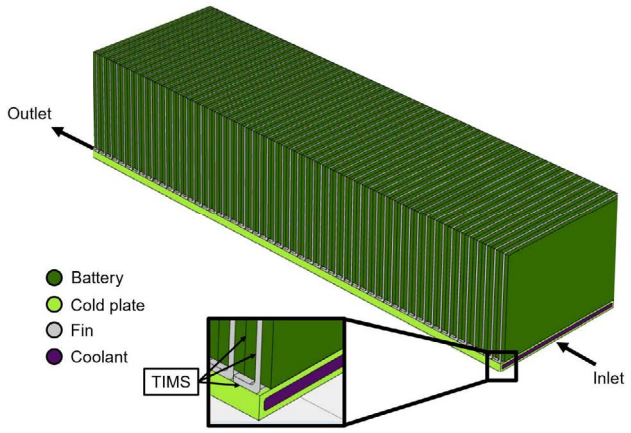

Fig 2: Constructed battery pack thermal model.

C. Co-simulation framework

To establish a co-simulation framework, Modelica and COMSOL must be made to communicate and simulate across a shared simulation time space. A java-based shared simulation server application is utilized [12], TISC, which acts as an intermediary that each separate simulation can connect and synchronize to. This coupling has been studied previously to pass of initialization conditions from Modelica to COMSOL and then back again as they simulate across discrete time [18]. A diagram of this process is shown in Fig 3.

The variables passed back and forth in this scenario are the heat generation inside of the battery module, temperature at discrete points inside the pack which are used to calculate the battery aging, and the coolant flow temperatures. For the purposes of this study, the battery is subdivided into six battery bundles whose values of heat generation are calculated in Modelica, passed to COMSOL, and then the predicted temperature distribution passed back. Additionally, the inlet temperature of the coolant to the battery module is passed from Modelica to COMSOL, and the outlet temperature is sent back.

Starting at point 1, Modelica initializes the simulation by transferring initial conditions to COMSOL via the shared simulation server which include the fluid flow rate through the module, inlet temperature to the coldplate, and heat generation inside the discretized battery pack. COMSOL then simulates the battery pack from points 2 to 3 for a prescribed time step and stops once that time is reached. The shared server then initiates the simulation in Modelica, which then simulates through the same time step from points 4 to 5. During this simulation, the values for variables passed from COMSOL, temperature of each battery bundle and outlet temperature of the module cold plate are held constant. Once Modelica reaches the end of the timestep these values are updated to be the same as the COMSOL model at point 5. Modelica then re-initializes the COMSOL simulation and the pattern continues till the end of the simulation at point 6.

For long-range BEV simulations, these interconnections require newly developed schemes for active control of the co-simulation step size, stop/start of the parameterized velocity profile, and control of the power demand from the battery in charging versus discharging conditions. These additional co-simulation controls are described in the following subsections.

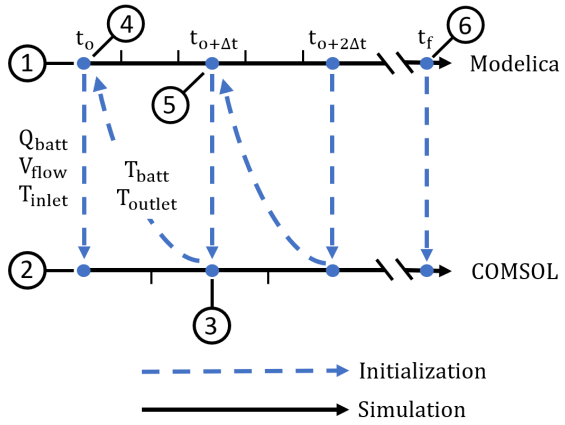

Fig 3: Outline of co-simulation process with information flow between the two simulations.

D. Derivative-controlled adaptive step size

Adaptive control of the co-simulation step size is motivated from the need to reduce the simulation time in response to complex velocity profiles that typically contain dramatic changes in vehicle velocity. For example, long periods of constant speed can tolerate large step sizes before exchanging variables between the co-simulations, while rapid changes in velocities during other portions of the velocity profile require much smaller step sizes to maintain a quantifiable and controllable level of accuracy. A scheme is developed that uses the derivative of a key independent control variable to determine the step size. This 'adaptive step size controller' is shown in Fig 4.

Examining the structure of the controller an independent variable, in this case the vehicle velocity, is input and the absolute value of its derivative is fed into an interpolation table that specifies the corresponding time step. For the application to a vehicle system, this table relates the acceleration, a_{1-N}, to the appropriate time step for co-simulation, Δt_{1-N} . As the acceleration of the vehicle increases, the time step output decreases based on the table. Time-shifted values of the velocity, $v_{\Delta t}$, simultaneously input into the controller to look forward and observe the velocity profile for future acceleration events. If the controller observes one of these events and it occurs after the end of the current time step, then the next time step is set as the difference between the time that event takes place and the end of the current time step. If that event happened in the past, then the time step is set by the original table output. In this way, the time step can be adjusted for acceleration events. An additional flag can be set to detect the ending of the simulation and set the time step such that the co-simulation ends appropriately once the final time is reached.

The response of the adaptive control scheme is illustrated in Fig 5 for an arbitrary velocity input profile. Briefly, at 16 sec there is an acceleration. From starting step size of 10 sec, the controller looks forward in time at this acceleration event and reduces the step size such that the co-simulation simulates only up to the event, and then switches to a much lower time step during the acceleration. Without a forward temporal scheme, the assigned initial step size would have missed a sizable period of acceleration from 16 to 20 sec. This adaptive behavior continues throughout the cycle, for example, at 30 sec as the vehicle's

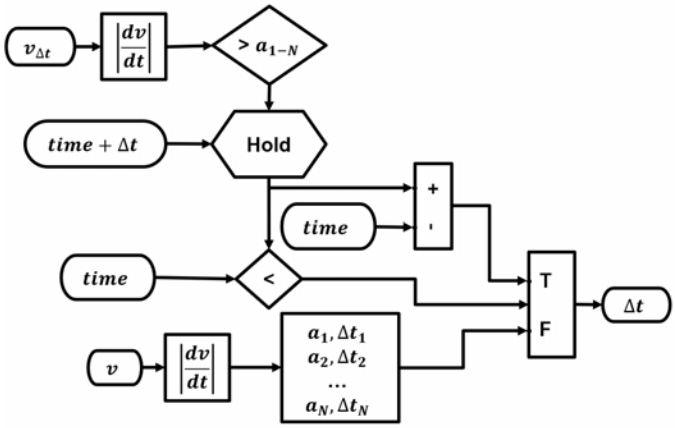

Fig 4: Derivative-based adaptive step size controller.

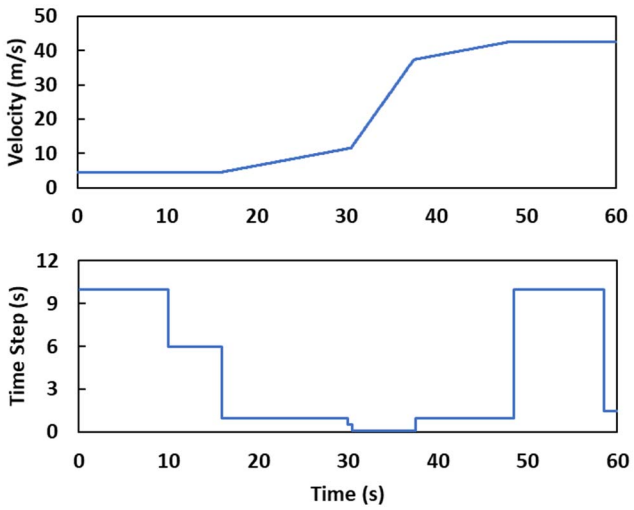

Fig 5: Plot demonstrating of the effect of the input velocity on the derivative-controlled adaptive time step size.

acceleration increases further. As the acceleration decreases later in the velocity profile, the step size adapts without any such adjustments because the time steps happen to align directly with the next time step. Finally, the end of the arbitrary velocity profile at 60 s is anticipated by the controller and the simulation ends correctly with an adjusted final timestep.

An appropriate discretization for the time step size for the actual simulations is determined using a multi-cycle test (MCT) protocol as a benchmarking case for the algorithm. The specific MCT velocity profile was detailed in our previous work [9, 10] and the velocity schedule is shown later in Fig 9a. This velocity is input into the algorithm established for controlling the co-simulation time step as the control variable. The input velocity error is then characterized in two ways: a comparison of the current true velocity and the co-simulated velocity, and a comparison of the integrated range from the co-simulation (TISC) and true velocity (SIM), calculated respectively as.

$$Error(\%) = \frac{v_{SIM} - v_{TISC}}{v_{SIM}} * 100\% \quad (5)$$

$$Range = \int_{t_0}^{t_f} v dt \quad (6)$$

In this way, an instantaneous and cumulative error metrics are established, and the choice of time step discretization ("Disc" in column one in Table 2) parameters in the co-simulation algorithm can be varied to characterize the error. For the instantaneous error the number of simulation points that fall below 10% and 100% are counted. The total number of points, as well as those counted and their percentage of the total, are shown in columns two to four in Table 2. Finally, the integrated ranges of the simulated and co-simulated velocity profiles are shown in the columns labeled SIM and TISC respectively with the difference between these reported in the final column. The results for a parametric investigation of co-simulation parameters are shown in Table 2.

Examining the results for the different step sizes, several trends become apparent. First, looking at the 10 s discretization compared to the 20 s one, is that as the largest allowable step size increases, so does the instantaneous error inside of the

Table 2: Investigation of co-simulation algorithm parameters for discretization of the time steps (Disc), total simulation points (Points), number of points with instantaneous error below 10% and 100%, and the integrated range of the simulation and co-simulation (SIM and TISC) with the difference between the ranges $\Delta(km)$.

Disc	Points	10%	100%	SIM (km)	TISC (km)	Δ(km)
10s	78263	65938 (84.3%)	75334 (96.3%)	318.927	318.762	-0.165
20s	76619	61226 (79.9%)	71907 (93.9%)	318.927	319.055	0.128
10, 5, 1s	79999	72120 (90.5%)	76966 (97.3%)	318.927	317.964	-0.963
10, 5, 2s	79615	68900 (86.5%)	77559 (97.4%)	318.927	318.822	-0.105
10, 7, 4, 1s	81805	70654 (86.4%)	79242 (97%)	318.927	318.348	-0.578

simulation. Second, comparing 20 s to 10, 5, 1 s, as the smallest allowable value of step size discretization decreases the instantaneous error as the number of points below 10% and 100% error improves by nearly 10% and 4%, respectively, at the cost of cumulative range errors. This then is counteracted by reducing the skewness of the discretization from a ratio of 10 in the third case to 5 in the fourth case, achieving better range results than the static first and second case counterparts with the same value of the largest step size. Finally, an increased discretization to four time step values in the last case shows that while maintaining the same level of skewness the static error can be improved while performing worse in dynamic error. For the purposes of simulations presented in this work the discretization of 10, 5, 2s is chosen.

E. Charge and discharge control

With the goal of establishing a lifetime simulation framework that considers both charging and driving scenarios, logic is developed for switching between charging and discharging modes and outputting the appropriate battery charging state as a function of battery state of charge (SOC). End of charge (EOC) and end of discharge (EOD) conditions are established at 0.98 and 0.2, respectively. The charging protocol is constant current constant voltage (CC-CV). The logic for this 'continuous charge and discharge controller' is presented in Fig 6.

The controller requires an initialization, either a 1 for discharging mode or a 0 for charging mode. If the EOD condition is reached a boolean test comparing the current SOC to the EOD moves from false to true, a negative 1 is then added to a continuous sum and switches the sum output from 1 to 0. This triggers a switch from discharging current to charging current. In the same way, if the EOC condition is reached, a 1 is added to the sum and the current switches. The switching binary value represents a charge/discharge binary value (CD) which is used to turn off key thermal system components according to the logic laid out in Section A.

The 'velocity profile controller' logic for allowing continuous simulation with the stopping and resumption of the velocity profile at the correct moments, is outlined in Fig 7. With an input of the CD binary, the controller looks for times when the vehicle is switching from discharging to charging.

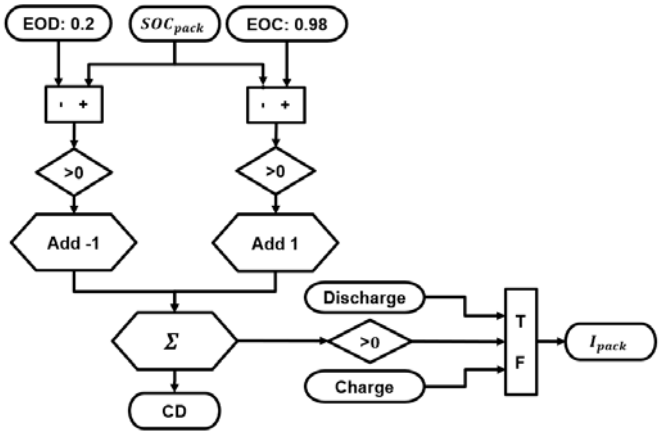

Fig 6: Continuous charge and discharge controller with the input of pack state of charge (SOC) and outputs of charge/discharge binary and battery pack current.

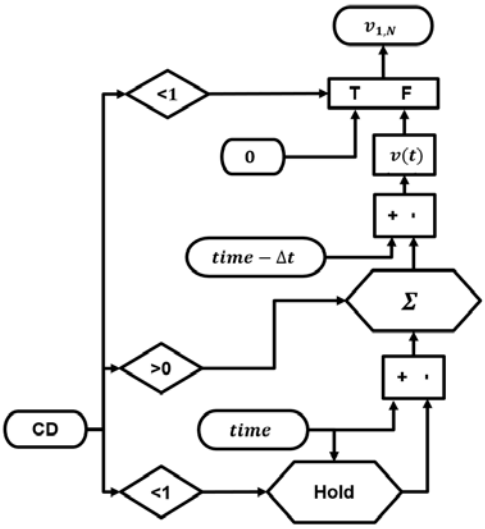

Fig 7: Velocity profile controller for continuous simulation with an input of the charge/discharge (CD) binary and an output of the appropriate velocity profile.

When it does, the system records that time and measures the difference between the current simulation time and when it began charging. Once the system detects that charging has ended, the CD binary switching from 0 to 1, and the time that the vehicle spent charging is subtracted from the input to the velocity profile function. In this way, the velocity profile is appropriately shifted based on the total time spent charging without a priori knowledge of the exact time needed for charging.

A summary of the full systems interconnections is shown in Fig 8. Demand currents and the battery SOC are passed to the battery charge/discharge controller, which determines if the vehicle is in charging or discharging mode. The current mode is then output as a binary number to control the starting and stopping of key thermal system components as well as the vehicle velocity throughout the cycle. The velocity profile controller then starts and stops the vehicle and outputs time shifted velocity profiles to the adaptive step size controller. These velocity profiles are used in the adaptive step size controller to set an appropriate co-simulation step size by observing the current vehicle acceleration and observing for acceleration events. This reduces dynamic error in the velocity profile while allowing for large time step sizes throughout the co-simulation. These step sizes are input into the battery model which passes discretized heat generation, flow rate, and the inlet temperature of the battery cold plate to the isothermal flow model. This battery submodel then passes back the resulting temperature distribution inside of the battery pack as well as the temperature at the outlet of the cold plate to the system model. Coulomb counting inside of the battery model tracks the pack SOC which then closes the loop on the novel co-simulation control logic developed herein.

Results

The velocity profile used as an input into the simulation is the MCT methodology [19] which combines transient velocity profiles with high constant speed portions to quickly drain the battery until a second round of transient velocity profiles examine low state of charge system performance. This velocity profile is then coupled with intermediate periods of fast charging. The initial SOC is set as 80% and the velocity profile is run until the system reaches the 20% EOD condition. Charging then occurs at a 5C rate up to the EOC condition of 98%. During charging, the battery is protected from overpotential via a CC-CV charging profile with 420 V set as the maximum pack value. The goal this simulation is to examine the implementation of the novel co-simulation scheme developed and to get an initial result for fast charging of a long-range BEV.

The ambient temperature is set to 35 °C so that the vehicle begins in discharge and cooling mode with the previously outlined TMS operation. The cabin setpoint is set to 18 °C with an inlet temperature of 14 °C. The ambient solar irradiation is set to 800 W/m^2 direct and 600 W/m^2 diffuse. The battery cooling setpoint is 35 °C with a coolant inlet of 30 °C.

With the specific input parameters set up, the co-simulated velocity cycle is shown in Fig 9a. Overall, the simulation runs for 48 hr to simulate ~4 hr of time. Note that this velocity profile is the actual output of the co-simulation algorithm that results from the vehicle stopping to charge. At ~12,200 s, the battery hits the EOD condition, and the velocity of the vehicle is ramped down to 0 m/s over 20 s. Then for the next 600 s the battery is charged at a 5C rate. This is confirmed when examining the battery pack SOC plotted over the same period in Fig 9b.

Following the initial transient velocity schedule, most of the battery drain occurs across the constant speed portion of the velocity profile starting at 4300 s until the EOD conditions

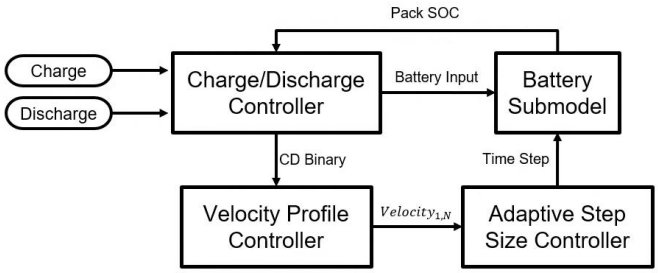

Fig 8: Overall co-simulation control algorithm.

trigger the charging cycle to occur at 12,220 s. Once the charging cycle completes at 12,872 s, the high constant speed cycle resumes and transitions into the final transient velocity profile mimicking the first period of the cycle except that now the cabin has been sitting unconditioned for the charge cycle.

The response of key thermal system control points is shown in Fig 9c. Beginning during the charging period, the cabin conditioning is disabled, and the cabin mean air temperature increases to ~58 °C until the end of the charge cycle. The compressor inside of the TMS controls the battery inlet temperature to its setpoint target, switching between the system control objectives successfully. Once the charging period ends at 13,000 s, the control objectives switch back and the cabin mean temperature is controlled to its setpoint. At this point the cabin fan turns back on, resuming airflow at the previous speed it was shutoff at for the start of the charging cycle. Because the cabin has a mix of 30% fresh air circulating through the system, the cabin quickly begins to cool back to its setpoint. However, once the cabin cools below the ambient temperature, its cooling rate slows as the system, starved of capacity from cooling the battery at the same time, fails to reach its setpoint for 1,600 s after the resumption of driving. This should be addressed in further iterations of control logic which better balance the battery pack and cabin cooling demand and through an increase in system capacity.

Examining next the performance of the battery pack thermal model, Fig 9d plots the average temperatures of each of the six battery bundles. Immediately apparent is that over discharge period, the battery temperature is generally well-controlled to below the 35 °C set point. Yet a moderate temperature difference inside of the pack occurs due to the streamwise heating of the coolant in the cold plate, which would contribute to non-uniform aging over the vehicle life. Once the charging cycle begins, the temperature inside of the battery pack begins to increase, peaking at ~35 °C, just as the charging cycle is ending. Once the charging period ends, each battery module is again controlled back toward its setpoint with decreasing temperature difference inside the pack along the flow path, indicating a high caloric resistance and a hard limit of the cooling solutions performance at the given conditions. This shows that the cooling loads of the cabin and battery are coupled together causing excessive battery aging in the final battery module and delayed response in the cabin conditioning.

IV. Conclusions

A comprehensive long-range BEV co-simulation framework encompassing adaptive control of co-simulation step sizes, continuous battery charge and discharge controllers, and velocity profile control is developed. The thermal system model includes all relevant power electronics, cabin, and battery thermal management. The thermal system model is uniquely coupled to a finite volume simulation of the battery module allowing for the resolution of battery temperature distribution while considering both discharge during the drive cycle and interspersed fast charging scenarios. The performance of the co-simulation control scheme is quantified by evaluating the accuracy of the instantaneous vehicle velocity and cumulative range; errors in these metrics are shown to be inversely related to the co-simulation time step size. The novel co-simulation control schemes are collectively demonstrated and discussed in the context of a case study on long range BEV TMS

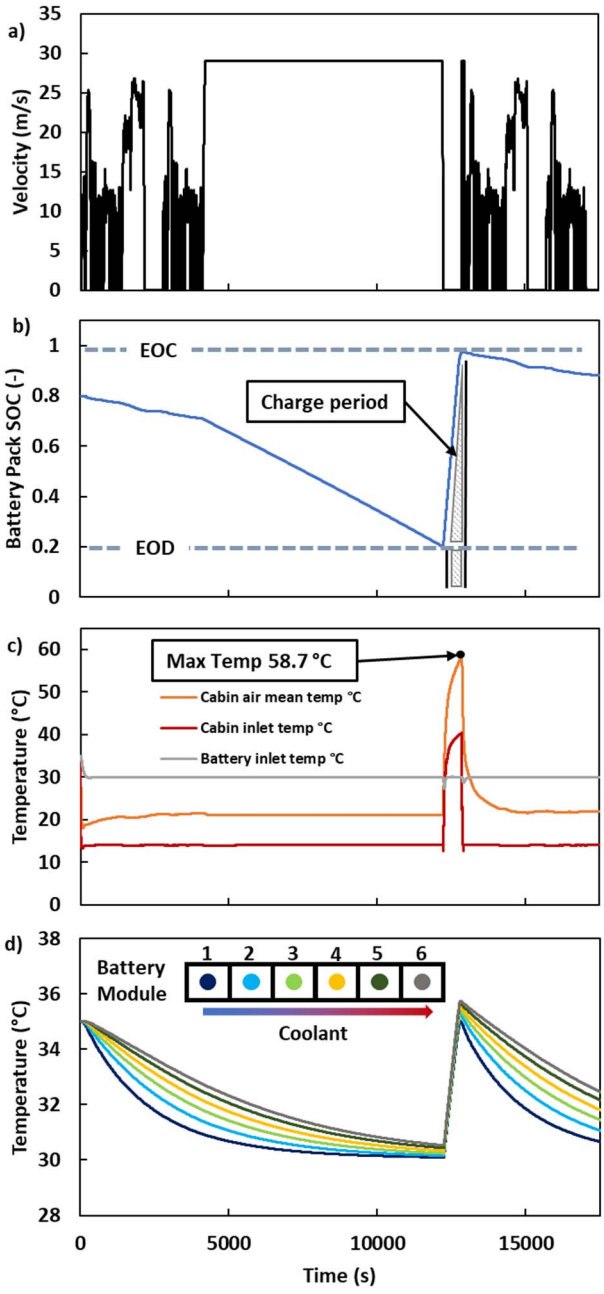

Fig 9: Plotted co-simulation results for: a) simulated velocity profile accounting for discharging followed by periods of fast charging; b) battery pack state of charge (SOC) plotted across the continuous charge-discharge long range cycle; c) response of cabin mean temperature, cabin inlet temperature, and battery inlet temperature across the continuous charge-discharge long range cycle; and d) average temperatures of each battery bundle in the pack across the continuous charge-discharge long range cycle.

performance across a continuous charge-discharge cycle, where the drive cycle follows an MCT methodology. In this study the active control of the co-simulation step size leads to low dynamic error and reduced cumulative range error. The vehicle system responds appropriately to complex boundary conditions,

handling the switching of modes of control between charging and discharging seamlessly. The integration of a high-fidelity finite volume submodel does increase simulation time but allows for the resolution of temperature differences inside of the designed battery module in response to transient control system response and boundary conditions. Future work will establish a technoeconomic framework using this model to assess TMS investments on the resulting lifetime battery aging, energy usage, and trip efficiency.

ACKNOWLEDGMENT

Financial support for this work provided by members of the Cooling Technologies Research Center, a graduated National Science Foundation Industry/University Cooperative Research Center at Purdue University, is gratefully acknowledged. The authors would like to acknowledge members of the Technical University of Braunschweig, Michael Steeb and Ingo Frohböse, for their support in providing access to the Modelica libraries.

REFERENCES

[1] J. Kim, J. Oh and H. Lee, "Review on battery thermal management system for electric vehicles," *Applied Thermal Engineering,* vol. 149, pp. 192-212, 2018.

[2] J. Nonneman, I. Trjollyn, N. Clarie, S. Weckx, P. Sergeant and M. D. Paepe, "Model-Based Comparison of Thermo-Hydraulic Performance of Various Cooling Methods for Power Electronics of Electric Vehicles," in *2018 17th IEEE Intersociety Conference on Thermal and Thermomechanical Phenomena in Electronic Systems (ITherm)*, San Diego, 2018.

[3] Z. Zhang, J. Wang, X. Feng, L. Chang, Y. Chen and X. Wang, "The solutions to electric vehicle air conditioning systems: A review," *Renewable and Sustainable Energy Reviews,* vol. 91, pp. 443-463, 2018.

[4] G. Titov and J. A. Lustbader, "Modeling Control Strategies and Range Impacts for Electric Vehicle Integrated Thermal Management Systems with MATLAB/Simulink," *SAE Technical Paper Series,* 2017.

[5] B. Yu, J. Yang, D. Wang, J. Shi and J. Chen, "Energy consumption and increased EV range evaluation through heat pump scenarios and low GWP refrigerants in the new test procedure WLTP," *International Journal of Refrigeration,* vol. 100, pp. 284-294, 2019.

[6] M. Jafari, A. Gauchia, S. Zhao, K. Zhang and L. Gauchia, "Electric Vehicle Battery Cycle Aging Evaluation in Real-World Daily Driving and Vehicle-to-Grid Services," *IEEE TRANSACTIONS ON TRANSPORTATION ELECTRIFICATION,* vol. 4, no. 1, pp. 122-134, 2018.

[7] J. Li, T. Huber and C. Beidl, "Predictive Multi-Objective Operation Strategy Considering Battery Cycle Aging for Hybrid Electric Vehicles," *SAE International Journal of Alternative Powertrains,* vol. 7, no. 3, pp. 217-232, 2019.

[8] R. Du, X. Hu, S. Xie, L. Hu, Z. Zhang and X. Lin, "Battery aging- and temperature-aware predictive energy management for hybrid electric vehicles," *Journal of Power Sources,* vol. 473, p. 228568, 2020.

[9] T. J. Shelly, J. A. Weibel, D. Ziviani and E. A. Groll, "A Dynamic Simulation Framework for the Analysis of Battery Electric Vehicle Thermal Management Systems," in *19th IEEE Intersociety Conference on Thermal and Thermomechanical Phenomena in Electronic Systems (ITherm)*, Orlando, 2020.

[10] T. J. Shelly, J. A. Weibel, D. Ziviani and G. A. Eckhard, "Comparative analysis of battery electric vehicle thermal management systems under long-range drive cycles," *Applied Thermal Engineering,* vol. 198, p. 117506, 2021.

[11] Dassault Systèmes, "What is Dymola?," Dassault Systèmes, Boston , 2019.

[12] TLK-Thermo GmbH, "TIL Suite," August 2020. [Online]. Available: https://www.tlk-thermo.com/images/tlk/content/presentations/TIL_Suite_EN_2020_August.pdf. [Accessed 21 July 2021].

[13] C. Multiphysics®, "COMSOL Multiphysics® v. 5.6," COMSOL AB, Stockholm, 2021.

[14] A. Cavallini, D. D. Col, L. Doretti, M. Matkovic, L. Rossetto, C. Zilio and G. Censi, "Condensation in Horizontal Smooth Tubes: A New Heat Transfer Model for Heat Exchanger Design," *Heat Transfer Engineering,* vol. 27, no. 8, pp. 31-38, 2006.

[15] K. E. Gungor and R. H. S. Winterton, "Simplified General Correlation for Saturated Flow Boiling and Comparison of Correlation with Data," *Chemical Engineering Research and Design,* vol. 65, no. 2, pp. 148-156, 1987.

[16] A. C. Arenas, S. Onori, Y. Guezennec and G. Rizzoni, "Capacity and power fade cycle-life model for plug-in hybrid electric vehicle lithium-ion battery cells containing blended spinel and layered-oxide positive electrodes," *Journal of Power Sources,* vol. 278, pp. 473-483, 2015.

[17] J. Cui, J. Wang, J. Weibel and L. Pan, "A compliant microstructured thermal interface material for dry and pluggable interfaces," *Internationl Journal of Heat and Mass Transfer,* vol. 131, pp. 1075-1082, 2019.

[18] A. Tosatto, F. Ochs and A. Dahash, "Co-Simulation of Dynamic Energy System Simulation and COMSOL Multiphysics," in *COMSOL Conference*, Cambridge, 2019.

[19] SAE, "Surface vehicle reccomended practice: Battery Electric Vehicle Energy Consumption and Range Test Procedure," SAE International, Evanston, 2017.